J. Phys. D: Appl. Phys. **46** (2013) 000000 (9pp) UNCORRECTED PROOF

Critical evaluation of analytical models for stochastic heating in dual-frequency capacitive discharges

S Sharma and M M Turner

National Centre for Plasma Science and Technology and School of Physical Sciences, Dublin City University, Dublin 9, Ireland

E-mail: sarvsarvesh@gmail.com

Received 1 March 2013, in final form 21 May 2013
Published
Online at stacks.iop.org/JPhysD/46

Abstract

Dual-frequency capacitive discharges are widespread in the semiconductor industry and are used, for example, in etching of semiconductor materials to manufacture microchips. In low-pressure dual radio-frequency capacitive discharges, stochastic heating is an important phenomenon. Recent theoretical work on this problem using several different approaches has produced results that are broadly in agreement insofar as scaling with the discharge parameters is concerned, but there remains some disagreement in detail concerning the absolute size of the effect for the case of dual-frequency capacitive discharges. In this work, we investigate the dependence of stochastic heating on various discharge parameters with the help of particle-in-cell (PIC) simulation. The dual-frequency analytical models are in fair agreement with PIC results for values of the low-frequency current density amplitude $J_{\rm lf}$ (or dimensionless control parameter $H_{\rm lf} \sim 5$) typical of many modern experiments. However, for higher values of $J_{\rm lf}$ (or higher $H_{\rm lf}$), new physical phenomena (like field reversal, reflection of ions, etc) appear and the simulation results deviate from existing dual-frequency analytical models. On the other hand, for lower $J_{\rm lf}$ (or lower $H_{\rm lf}$) again the simulation results deviate from analytical models. So this research work produce a relatively extensive set of simulation data that may be used to validate theories over a wide range of parameters.

AQ1 (Some figures may appear in colour only in the online journal)

1. Introduction

Good plasma uniformity, fast processing rates and damage-free characteristics are major requirements for plasma etching in modern industry. Anisotropy is also a critical process parameter in integrated circuit manufacturing and can be achieved using radio-frequency (RF) plasma etching. Single-frequency reactors have limitations, and in particular fail to provide an independent control of ion energy and ion flux. Hence dual-frequency capacitively coupled plasma (DF-CCP) system operated with two distinct power sources has been developed [1–4]. In ideal cases, the lower frequency ($\omega_{\rm lf}$) controls the sheath voltage i.e. ion bombarding energy while the higher frequency ($\omega_{\rm hf}$) can control the plasma density, i.e. the ion flux. Ohmic heating and stochastic heating are the two main electron heating mechanisms in capacitive discharges. Ohmic heating occurs in the bulk and sheath regions because of electron–neutral collisions, and stochastic (or collisionless) heating takes place at sheath edge because of the momentum transfer from high voltage moving sheath to electrons. While Ohmic heating dominates at relatively high pressures, stochastic heating is the dominant heating mechanism at low pressures (in the mTorr range) and is then expected to sustain the plasma. In low-pressure RF discharges, stochastic heating dominates and the power absorbed by electrons is given by

$$\bar{S}_{\rm stoc} \propto \omega_{\rm rf}^2 V_{\rm rf}. \tag{1}$$

The plasma density is approximately proportional to the stochastic heating [5], i.e.

$$n \propto \bar{S}_{\rm stoc}. \tag{2}$$

JNL: JPD PIPS: 465471 TYPE: PAP TS: NEWGEN DATE: 7/6/2013 EDITOR: MJ SPELLING: UK

This is also experimentally seen by Perret *et al* [6] and by Jolly and Booth [7]. Let us assume that the voltage amplitudes of low and high driving frequencies are $V_{\rm lf}$ and $V_{\rm hf}$, respectively. Now if one can satisfy the following condition

$$\omega_{\rm hf}^2 V_{\rm hf} \gg \omega_{\rm lf}^2 V_{\rm lf} \tag{3}$$

then the plasma density, i.e. the ion flux, is being controlled by $\omega_{\rm hf}$, the high-frequency source [8].

The mean ion bombarding energy $\xi_{\rm i}$ is equivalent to the total dc bias voltage across the collisionless sheath, in the absence of ion collisions. The sheath voltage is approximately equal to the applied RF voltage. For the dual-frequency case

$$\xi_{\rm i} \propto |V_{\rm hf} + V_{\rm lf}|. \tag{4}$$

For the case of

$$V_{\rm lf} \gg V_{\rm hf}, \tag{5}$$

the dc sheath voltage (i.e. mean ion bombarding energy) can be controlled by $V_{\rm lf}$. From equations (3) and (5), the condition for independent control of ion energy and ion flux is as follows [5]:

$$\frac{\omega_{\rm hf}^2}{\omega_{\rm lf}^2} \gg \frac{V_{\rm lf}}{V_{\rm hf}} \gg 1. \tag{6}$$

Lieberman *et al* [5] showed that $J_{\rm rf} \propto \omega_{\rm rf} V_{\rm rf}^{3/4}$. So if $J_{\rm rf}$ is the controlling parameter, equation (6) can be inverted by substitution of $V_{\rm rf}$. Thus, equation (6) indicates that $J_{\rm hf} \gg J_{\rm lf}$, where $J_{\rm lf}$ and $J_{\rm hf}$ are the low- and high-frequency current density amplitudes, respectively. Again equation (6) shows that even in the case when the first inequality is true, the collisionless heating and in consequence of that the ion density and ion flux are not completely independent of the applied low frequency, $\omega_{\rm lf}$. In DF-CCP, the higher frequency is superimposed on the lower frequency. The characteristic ratio of high frequency ($f_{\rm hf}$) to low frequency ($f_{\rm lf}$) is greater than 10 to minimize the coupling between low and high frequency. However, for the case of stochastic heating some form of coupling is assumed between the low- and high-frequency components. In the dual-frequency case, the total stochastic heating effect is a collective effect due to the presence of high-frequency sheath oscillating across a low-frequency sheath. Typically, the high frequencies and low frequencies are chosen to be $f_{\rm hf} \sim 27.12$–160 MHz and $f_{\rm lf} \sim 2$–13.56 MHz, respectively.

In the last few decades, the industrial application of RF discharges at low-pressures has increased, due to this it is important to understand the physical mechanism of stochastic heating. Stochastic heating in the case of low-pressure dual-frequency capacitive discharges has been studied by different analytical models [2, 8–15]. Turner and Chabert [12, 13] developed a fluid model for dual-frequency sheath, which is an extension of the kinetic-fluid approach of Gozadinos *et al* [16]. Kinetic treatment in which the current is conserved has been developed by Kaganovich [17] for the single-frequency case. He assumed an ion density with a step discontinuity at the plasma–sheath interface. This ion density model is a useful tool for the investigation of stochastic heating in single-frequency RF discharges, even though it is not realistic.

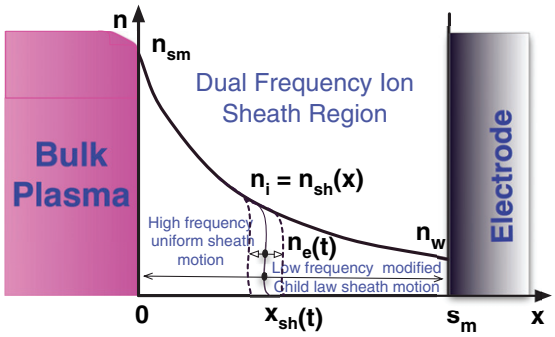

Figure 1. Schematic diagram of the dual-frequency capacitive sheath.

Kawamura *et al* [10] have extended the Kaganovich [17] model to the case of dual-frequency CCP, and have presented comparisons with particle-in-cell (PIC) simulations. We will further discuss this work in the next section.

In this paper, we discuss several different dual-frequency analytical models for stochastic heating in section 2. The dependence of stochastic heating on various discharge parameters is studied with the help of PIC simulation in section 3. The comparison of stochastic heating yielded by the higher and lower frequency acting alone and by the superposition of both frequencies is studied in section 4. Finally we summarize our conclusions and discuss the results in section 5.

2. Dual-frequency analytical models

There are different analytical models which predict the stochastic heating in the case of dual-frequency CCP discharges. Figure 1 is a schematic representation of DF-CCP, illustrating the mechanism of low-frequency sheath motion and high-frequency sheath motion. It is clear from this figure that a low-frequency 'modified Child law sheath' is coupled with high-frequency uniform sheath motion. Ions of mass $m_{\rm i}$ enter the ion-sheath boundary at $x = 0$ with a velocity of the order of the Bohm speed $u_{\rm B} = (k_{\rm B} T_{\rm e}/m_{\rm i})^{1/2}$ determined by the electron temperature $T_{\rm e}$, are further accelerated within the sheath by the sheath potential, and finally strike the electrode at $x = s_{\rm m}$ with high energies. The ion motion is considered collisionless. Since the ion velocity increases as the electrode is approached, due to ion flux conservation, the ion density $n_{\rm sh}(x)$ decreases continuously from its maximum value $n_{\rm sm}$ (at the ion-sheath–plasma boundary) to its minimum value $n_{\rm w}$ (at the electrode) (see figure 1). So in a self-consistent discharge, the plasma density is not uniform. In figure 1, $x_{\rm sh}(t)$ is the instantaneous position of the oscillating electron sheath edge. The electron sheath edge oscillates between the wall at $x = s_m$ and the ion-sheath boundary at $x = 0$. An analytical model based on kinetic treatment for the calculation of stochastic heating in dual-frequency CCP has been developed by Kawamura *et al* [10]. This model is an extension of the Kaganovich [17] model for stochastic heating calculation for the single-frequency CCP case. We briefly describe the dual-frequency analytical model given by Kawamura *et al* [10]. The dual-frequency discharges

were driven by current

$$J_{\rm rf}(t) = J_{\rm hf}\ \sin\omega_{\rm hf}t + J_{\rm lf}\ \sin\omega_{\rm lf}t, \tag{7}$$

where $J_{\rm hf}$, $J_{\rm lf}$ are high- and low-current density amplitudes and $\omega_{\rm lf}$, $\omega_{\rm hf}$ are applied low and high angular frequencies, respectively. In this dual-frequency model, a high-frequency ($f_{\rm hf}$) uniform sheath motion is superimposed on a low-frequency ($f_{\rm lf}$) 'modified Child law sheath' motion. Here the ion density is nearly constant for high-frequency sheath motion, hence stochastic heating expression calculated from *uniform ion density* model given by Godyak [18] can be used. For the case of low-frequency cycle, at each phase $\phi_{\rm lf} = \omega_{\rm lf}t$, the high-frequency electron oscillation occurs at the ion-sheath density $n_{\rm sh}(\phi_{\rm lf})$ which is the modified Child law sheath density (detailed derivation in Lieberman [19]). In DF-CCP, a positive net power deposition for a collisionless RF sheath driven by a sinusoidal current $J_{\rm rf}(t)$ (equation (7)) is given by

$$S_{\rm stocDF} = \tfrac{1}{2}m_{\rm e}\bar{v}_{\rm e}n_{\rm sm}u_{\rm bh}^2F(H_{\rm lf}) \tag{8}$$

where

$$F(H_{\rm lf}) = \frac{\pi H_{\rm lf}}{4} - 1 + \frac{1}{\pi}\int_0^{\pi}\frac{{\rm d}\phi}{1 - H_{\rm lf}N(\phi_{\rm lf})}. \tag{9}$$

Here, $u_{\rm bh} = J_{\rm hf}/(en_{\rm sm})$ is the velocity amplitudes of the high-frequency bulk motion. Other parameters are as follows: $\bar{v}_{\rm e}$ is the mean electron thermal velocity, i.e. $\bar{v}_{\rm e} = [8k_{\rm B}T_{\rm e}/(\pi m_{\rm e})]^{1/2}$, electron mass is $m_{\rm e}$ and density at the ion-sheath edge is $n_{\rm sm}$. Here the controlling parameter $H_{\rm lf}$ can be interpreted as a

$$H_{\rm lf} = \frac{J_{\rm lf}^2}{\pi\varepsilon_0 k_{\rm B}T_{\rm e}n_{\rm sm}\omega_{\rm lf}^2} \tag{10}$$

and $N(\phi_{\rm lf})$ is defined as

$$N(\phi_{\rm lf}) \equiv -\left(\frac{3}{8}\sin 2\phi_{\rm lf} - \frac{1}{4}\phi_{\rm lf}\ \cos 2\phi_{\rm lf} - \frac{1}{2}\phi_{\rm lf}\right). \tag{11}$$

In equation (9), the last integral can be solved numerically. A good parametric fit is

$$F(H_{\rm lf}) \approx \frac{H_{\rm lf}(1 + \pi H_{\rm lf}/4)}{H_{\rm lf} + 2.2}. \tag{12}$$

So equation (8) can be re-written in terms of high-frequency and low-frequency contributions, as follows:

$$S_{\rm stocDF} = \underbrace{\frac{1}{2}m_{\rm e}\bar{v}_{\rm e}\frac{J_{\rm hf}^2}{e^2n_{\rm sm}}}_{\textbf{High-frequency part}} \times \underbrace{\left(1 + \frac{\pi}{4}H_{\rm lf}\right)\left(\frac{H_{\rm lf}}{H_{\rm lf} + 2.2}\right)}_{\textbf{Low-frequency part}}. \tag{13}$$

The above expression makes clear that in a DF-CCP, the stochastic heating is the product of both high- and low-frequency processes rather than the additive effect of two single-frequency processes individually. Again, neglecting the bulk oscillation by setting $u_{\rm bh} = 0$, which gives the upper limit of stochastic heating, $S_{\rm stocUL}$, is defined as

$$S_{\rm stocUL} = \frac{1}{2}m_{\rm e}\bar{v}_{\rm e}n_{\rm sm}u_{\rm bh}^2\left(1 + \frac{\pi H_{\rm lf}}{4}\right). \tag{14}$$

Finally, normalized stochastic heating for a dual-frequency CCP, $\zeta(H_{\rm lf})$, can be obtained by dividing equation (8) by equation (14) to find

$$\zeta(H_{\rm lf}) \equiv \frac{S_{\rm stocDF}}{S_{\rm stocUL}} = \frac{F(H_{\rm lf})}{1 + \pi H_{\rm lf}/4} \approx \frac{H_{\rm lf}}{H_{\rm lf} + 2.2}. \tag{15}$$

It is important to note that equation (15) looks like the stochastic heating expression for single-frequency analytical model given by Kaganovich *et al* [21], since dual-frequency stochastic heating model developed by Kawamura *et al* [10] is just an extension of the single-frequency stochastic heating model developed by Kaganovich *et al* [21].

Another model based on fluid equations was developed by Turner and Chabert [12] to calculate stochastic heating for DF-CCP. Heating yielded by a kinetic-fluid model in the dual-frequency case is given by

$$S_{\rm stocT} = \frac{\pi}{16}m_{\rm e}n_{\rm sm}\bar{v}_{\rm e}(u_{\rm bl}^2 + 1.1u_{\rm bh}^2)F_T(H_{\rm lf}), \tag{16}$$

where $u_{\rm bl} = J_{\rm lf}/en_{\rm sm}$ is the velocity amplitude of low-frequency motion of electrons in the bulk plasma. Neglecting the contributions of $u_{\rm bl}$ we obtain

$$S_{\rm stocT} \approx \frac{1.1\pi}{16}m_{\rm e}n_{\rm sm}\bar{v}_{\rm e}u_{\rm bh}^2F_{\rm T}(H_{\rm lf}), \tag{17}$$

where the function $F_{\rm T}$ is estimated by a parametric fit, shown below

$$F_{\rm T}(H_{\rm lf}) = \frac{36H_{\rm lf}}{55 + H_{\rm lf}}. \tag{18}$$

Finally the normalized stochastic heating can be written by dividing equation (17) from (14)

$$\zeta_{\rm T}(H_{\rm lf}) \equiv \frac{S_{\rm stocT}}{S_{\rm stocUL}} \approx \frac{4.95\pi H_{\rm lf}}{(55 + H_{\rm lf})(1 + \pi H_{\rm lf}/4)}. \tag{19}$$

These analytical results were also checked by specialized PIC simulation in which the ions were held fixed [12].

3. Simulation results

Kawamura *et al* [10] used mobile ion PIC simulation in argon plasma to benchmark the dual-frequency analytical model (discussed in previous section) for stochastic heating. The dual-frequency analytical model given by Kawamura *et al* [10] is an extension of the Kaganovich [17] model of the single-frequency CCP case, and is based on hard wall approximations. In kinetic theory and the kinetic-fluid approach [12], it is not easy to see how to avoid the heuristic elements in a mathematically tractable fashion. The other possibility is that a better sheath model than that of Lieberman [19] is needed, in particular, because the representation of the electron sheath edge as a step function may be one of the less satisfactory approximations that feature in all models [23, 24]. In a further step to improve these models, the results should be compared with simulations and experiments. Simulations are the only choice because there are no experiments that serve the purpose. In this regard, it is to be noted that all theoretical models agree on the form represented by the equation (15)

and it makes easier to compare the theoretical models and the models with simulation results. Moreover, assuming that all the theoretical models are accurate in agreeing on the form represented by equation (15), allows one to ignore differences between the theories and choose $\zeta(H_{\rm lf})$ in line with simulation data. Kawamura *et al* [10] followed the same approach in their recent work.

Here dual-frequency discharges were driven by the RF current defined in equation (7). The controlling parameters for stochastic heating in the dual-frequency case are $J_{\rm lf}$, $J_{\rm hf}$, $\omega_{\rm lf}$, $\omega_{\rm hf}$, $T_{\rm e}$ and $n_{\rm sm}$. Parameters used by Kawamura *et al* [10] for their PIC simulations are as follows: $p = 15$ mTorr, $f_{\rm hf} = 32$ MHz and $f_{\rm lf} = 2$ MHz. The high- and low-current density amplitudes are varied from $J_{\rm hf} = 8$ to 16 A m^{-2} and $J_{\rm lf} = 2$ to 4 A m^{-2}, respectively, so the ratio of $J_{\rm hf}/J_{\rm lf} = 4$ in each set of simulation. The electron temperature $T_{\rm e} = 2$ eV here. Equation (10) indicates that $H_{\rm lf}$ depends on $J_{\rm lf}$ and $n_{\rm sm}$. The value of $J_{\rm lf}$ increases from 2 to 4 A m^{-2} and $n_{\rm sm}$ varied from 5×10^{14} to 1.4×10^{15} m^{-3} simultaneously, $H_{\rm lf}$ is varied from 5.0 to 8.2. Kawamura *et al* [10] concluded that simulation data (PIC results) are in good agreement with analytical model given by equation (15). On these grounds, equation (15) is the most appropriate formula. Here it is to be noted that the number of data points are rather small and large simulation database needs to be generated, that might give improved formula for stochastic heating.

As we have explained above, there are six scaling parameters (i.e. $J_{\rm lf}$, $J_{\rm hf}$, $\omega_{\rm lf}$, $\omega_{\rm hf}$, $T_{\rm e}$ and $n_{\rm sm}$) which control the stochastic heating. There are different ways to vary these parameters. We will discuss two of them for the applied *low* and *high RF*, $f_{\rm lf} = 1.695$ MHz and $f_{\rm hf} = 27.12$ MHz, in our simulations and investigate the validation of analytical models. We used semi-infinite PIC method, in which electrons and ions are injected at the left boundary using drifting Maxwellian velocity distributions, and particles incident on both boundaries from the plasma are absorbed. The ion flux is a boundary condition in this procedure. Under most—but not all—conditions, this has the effect of defining the ion density at the sheath edge, $n_{\rm sm}$. We note that an additional heating effect discussed in the literature, the so-called bounce resonance [5, 14, 25], cannot occur in this model, which simulates a sheath adjacent to a semi-infinite plasma. The simulation procedure is described in detail in [20]. In this work, the PIC simulation is conducted for current-driven argon discharges in which both electrons and ions were moved by the usual PIC method. Plasma is considered collisionless so there are no electron–neutral and ion–neutral collisions, etc. The ions and electrons are loaded initially and evolve with time until the self-consistent steady-state configuration is achieved. However, stochastic heating is known to occur predominantly near to the sheath edge. Therefore, we identify the sheath edge and calculate the stochastic heating over this region only. The method for calculating the analytical stochastic heating is described in Kawamura *et al* [10].

3.1. The first approach

In the first approach, benchmarking of the analytical model is the same as that used by Kawamura *et al* [10] where $H_{\rm lf}$ is calculated by varying $J_{\rm lf}$ and $n_{\rm sm}$ simultaneously. The ratio of $J_{\rm hf}/J_{\rm lf} = 8$ for each set of simulations. The parameter $\bar{v}_{\rm e}$ did not vary much with $J_{\rm lf}$ and stayed nearly constant, i.e. 1.058×10^6 m s^{-1}.

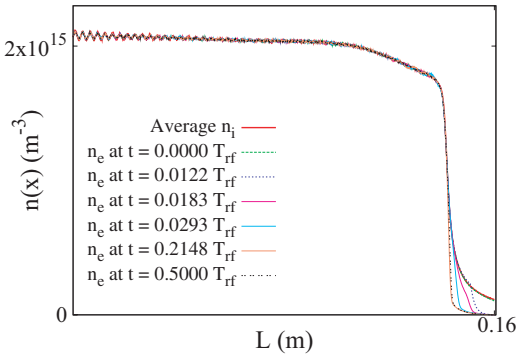

Figure 2. Averaged ion and snapshots of electron density profiles for the collisionless case in dual-frequency PIC simulation. The solid line represents the average ion density and the electron density is represented by dashed lines during different times of an RF period, i.e. $T_{\rm rf}$. Conditions: argon gas, $J_{\rm lf} = 4$ A m^{-2}, $J_{\rm hf} = 32$ A m^{-2}, $f_{\rm lf} = 1.695$ MHz, $f_{\rm hf} = 27.12$ MHz, $H = 6.77$, $T_{\rm e} = 2.5$ eV, $T_{\rm i} = 0.03$ eV at density 2×10^{15} m^{-3}.

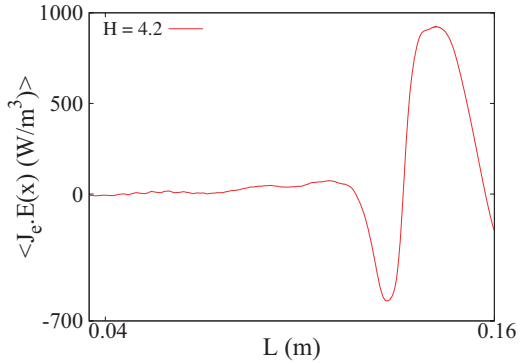

Figure 3. Self-consistent mobile-ion dual-frequency PIC simulation results for $\langle J_{\rm e}.E \rangle$ in the collisionless case. Conditions: argon gas, $J_{\rm lf} = 1.1$ A m^{-2}, $J_{\rm hf} = 8.8$ A m^{-2}, $f_{\rm lf} = 1.695$ MHz, $f_{\rm hf} = 27.12$ MHz, $H_{\rm lf} = 4.2$, $T_{\rm e} = 2.5$ eV, $T_{\rm i} = 0.03$ eV at density 3×10^{14} m^{-3}.

Figure 2 shows the averaged ion and snapshots of electron density profiles in the collisionless case. The ion-sheath density $n_{\rm sh}(x)$ decreases monotonically from a maximum density at the ion-sheath boundary to a minimum of $n_{\rm w} = 1.103 \times 10^{14}$ m^{-3} at the wall (or electrode). This is for argon gas at $J_{\rm lf} = 4$ A m^{-2}, $J_{\rm hf} = 32$ A m^{-2}, $H_{\rm lf} = 6.77$, $T_{\rm e} = 2.5$ eV, $T_{\rm i} = 0.03$ eV at the density 2×10^{15} m^{-3}.

The power deposition calculated by PIC simulation needs to be compared with that predicted by the dual-frequency analytical model given by Kawamura *et al* [10]. Figures 3 and 4 show the time-averaged local heating rate $\langle J_{\rm e}.E \rangle$ for $H_{\rm lf} \approx 4.2$ and 6.77 for the *density* of 3×10^{14} m^{-3} and 2×10^{15} m^{-3}, respectively. It is clear that the overall heating increases for higher $H_{\rm lf}$ because $H_{\rm lf}$ increases by increasing $J_{\rm lf}$. Figures 5 and 6 show the spatiotemporal profile of full $J_{\rm e}.E$ for the same cases. The stochastic heating phenomenon occurs near to the sheath edge. Figure 7 shows the variation of normalized stochastic heating $\zeta(H_{\rm lf}) \equiv S_{\rm stocDF}/S_{\rm stocUL}$

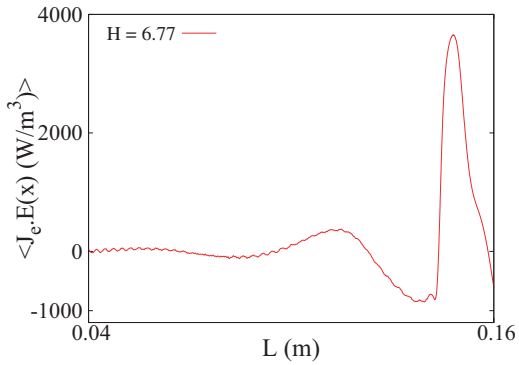

Figure 4. Self-consistent mobile-ion dual-frequency PIC simulation results for $\langle J_e.E \rangle$ in the collisionless case. Conditions: argon gas, $J_{lf} = 4\,\mathrm{A\,m^{-2}}$, $J_{hf} = 32\,\mathrm{A\,m^{-2}}$, $f_{lf} = 1.695\,\mathrm{MHz}$, $f_{hf} = 27.12\,\mathrm{MHz}$, $H_{lf} = 6.77$, $T_e = 2.5\,\mathrm{eV}$, $T_i = 0.03\,\mathrm{eV}$ at density $2 \times 10^{15}\,\mathrm{m^{-3}}$.

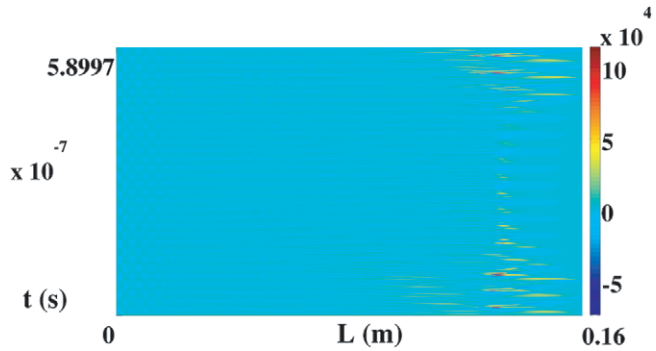

Figure 5. Spatiotemporal profile of $J_e.E$ for the same case as shown in figure 3 for the collisionless case. Conditions: argon gas, $J_{lf} = 1.1\,\mathrm{A\,m^{-2}}$, $J_{hf} = 8.8\,\mathrm{A\,m^{-2}}$, $f_{lf} = 1.695\,\mathrm{MHz}$, $f_{hf} = 27.12\,\mathrm{MHz}$, $H_{lf} = 4.2$, $T_e = 2.5\,\mathrm{eV}$, $T_i = 0.03\,\mathrm{eV}$ at density $3 \times 10^{14}\,\mathrm{m^{-3}}$.

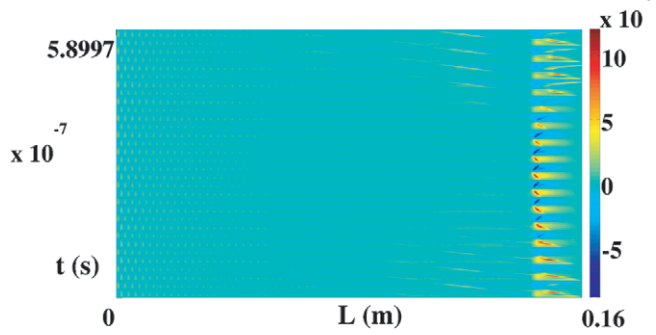

Figure 6. Spatiotemporal profile of full $J_e.E$ for the same case as shown in figure 4 for the collisionless case. Conditions: argon gas, $J_{lf} = 4\,\mathrm{A\,m^{-2}}$, $J_{hf} = 32\,\mathrm{A\,m^{-2}}$, $f_{lf} = 1.695\,\mathrm{MHz}$, $f_{hf} = 27.12\,\mathrm{MHz}$, $H_{lf} = 6.77$, $T_e = 2.5\,\mathrm{eV}$, $T_i = 0.03\,\mathrm{eV}$ at density $2 \times 10^{15}\,\mathrm{m^{-3}}$.

with respect to H_{lf}. The PIC simulation results (circles) are compared with the dual-frequency analytical model given by Kawamura *et al* [10]. Here $\zeta(H_{lf})$ given by equation (15) and the hard wall upper limit having $\zeta(H_{lf}) = 1$ (dashed line) are also indicated. Here the current drive amplitudes are varied from $J_{lf} = 0.5$ to $11.12\,\mathrm{A\,m^{-2}}$ and $J_{hf} = 4.0$ to $88.96\,\mathrm{A\,m^{-2}}$ at the corresponding densities of $n_{sm} \approx 1.1 \times 10^{14}$–$4 \times 10^{15}\,\mathrm{m^{-3}}$.

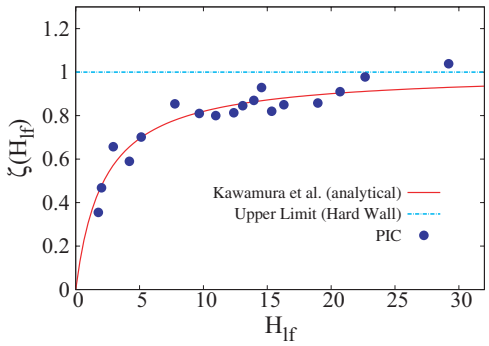

Figure 7. Normalized stochastic heating $\zeta(H_{lf}) \equiv S_{stocDF}/S_{stocUL}$ from the PIC simulation (circles), and the dual-frequency analytical model given by Kawamura *et al* [10] (solid line). The hard wall upper limit is also indicated (dashed line). Conditions: argon gas, $f_{lf} = 1.695\,\mathrm{MHz}$, $f_{hf} = 27.12\,\mathrm{MHz}$, $T_e = 2.5\,\mathrm{eV}$, $T_i = 0.03\,\mathrm{eV}$.

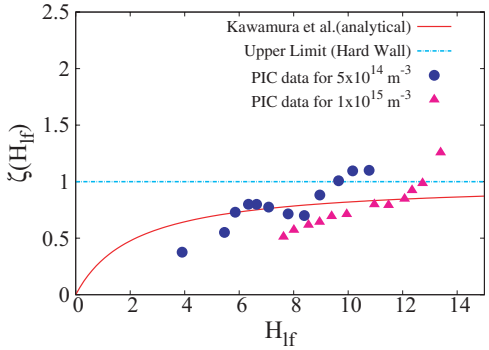

Figure 8. Normalized stochastic heating $\zeta(H_{lf}) \equiv S_{stocDF}/S_{stocUL}$ from the PIC simulation for two different densities, i.e. 5×10^{14} and $1 \times 10^{15}\,\mathrm{m^{-3}}$. The dual-frequency analytical model given by Kawamura *et al* [10] is represented by the solid line. The hard wall upper limit is also shown in the graph (dashed line). Conditions: argon gas, $f_{lf} = 1.695\,\mathrm{MHz}$, $f_{hf} = 27.12\,\mathrm{MHz}$, $T_e = 2.5\,\mathrm{eV}$, $T_i = 0.03\,\mathrm{eV}$.

So the ratio of $J_{hf}/J_{lf} = 8$. It is clear from figure 7 that the PIC data agree fairly well with the dual-frequency analytical model given by Kawamura *et al* [10] for the range of H_{lf}, i.e. $H_{lf} \approx 1.77$–29.2.

3.2. The second approach

In the second approach, the stochastic heating is investigated by keeping the density constant and varying the ratio of J_{hf}/J_{lf}, by changing the lower current density amplitude J_{lf}. We have investigated this point for two different densities, i.e. 5×10^{14} and $1 \times 10^{15}\,\mathrm{m^{-3}}$. The electron temperature T_e is 2.5 eV and ion temperature is at nearly room temperature, i.e. $T_i = 0.03\,\mathrm{eV}$. The parameter $\bar{v}_e = 1.058 \times 10^6\,\mathrm{m\,s^{-1}}$ stayed approximately constant. The applied lower and upper frequencies are 1.695 MHz and 27.12 MHz, respectively.

In figure 8, the normalized stochastic heating $\zeta(H_{lf}) \equiv S_{stocDF}/S_{stocUL}$ from the mobile-ion PIC simulations for two different densities, 5×10^{14} and $1 \times 10^{15}\,\mathrm{m^{-3}}$, is compared with the dual-frequency analytical model given by Kawamura *et al* [10]. Here $\zeta(H_{lf})$ given by equation (15) and the hard wall upper limit having $\zeta(H_{lf}) = 1$ (dashed line) is also indicated. In figure 8, circles and triangles show the normalized stochastic

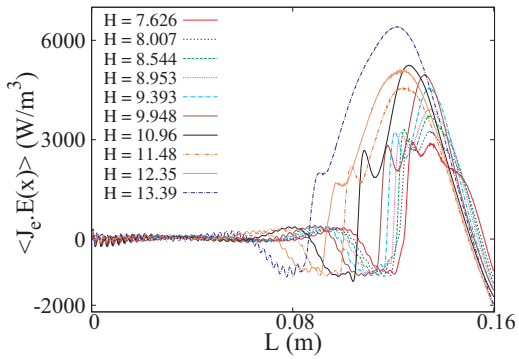

Figure 9. Self-consistent mobile-ion dual-frequency PIC simulation results for $\langle J_e.E\rangle$ in the collisionless case. Conditions: argon gas, $J_{lf} = 2.7$–$3.6\,A\,m^{-2}$, $J_{hf} = 26.4\,A\,m^{-2}$, $f_{lf} = 1.695\,MHz$, $f_{hf} = 27.12\,MHz$, $H_{lf} = 7.6$–13.4, $T_e = 2.5\,eV$, $T_i = 0.03\,eV$ at density $1 \times 10^{15}\,m^{-3}$.

heating calculated at densities $5 \times 10^{14}\,m^{-3}$ and $1 \times 10^{15}\,m^{-3}$, respectively. This graph indicates that the range of H_{lf} which fairly agrees with the dual-frequency analytical model given by Kawamura *et al* [10] is 5.8–9.0 and 9.4–12.35 for the densities of $5 \times 10^{14}\,m^{-3}$ and $1 \times 10^{15}\,m^{-3}$, respectively. In each case after the upper critical limit of H_{lf} (in which the analytical model agrees with the simulation) the stochastic heating increases rapidly. The following conclusions can be made from the above discussion. (i) At constant density the simulation results agree with the dual-frequency analytical model given by Kawamura *et al* [10] for a certain range of H_{lf}. (ii) For lower densities, the dual-frequency analytical model given by Kawamura *et al* [10] agrees with the simulation results for lower values of H_{lf}. Similarly, for higher densities, the dual-frequency analytical model agrees with the simulation results for higher values of H_{lf}, respectively.

Now we will study specific case of $1 \times 10^{15}\,m^{-3}$ in detail. Figure 9 shows the time-averaged local heating rate $\langle J_e.E\rangle$. Here by varying J_{lf} from 2.7 to $3.6\,A\,m^{-2}$, H_{lf} changes from 7.6 to 13.4. The current density amplitude for higher frequency (J_{hf}) is constant here, i.e. $26.4\,A\,m^{-2}$. This figure shows that for the value of $H_{lf} > 12.35$, stochastic heating increases rapidly. Here 12.35 is the upper critical limit of H_{lf}.

We have studied carefully the case $H_{lf} = 13.39$ and observed the signature of ion reflection here, as we encountered in the single-frequency case [22]. The rapid increase in heating is related to this ion reflection phenomena. Figure 10 shows the trajectory of ions in velocity phase space for the case of $J_{lf} = 3.6\,A\,m^{-2}$ and $J_{hf} = 26.4\,A\,m^{-2}$. Here the positive velocity indicates the direction towards the sheath (or electrode) and a negative velocity indicates the direction towards the bulk plasma, i.e. opposite to the sheath. The ion motion is collisionless within the sheath and the ions are accelerated by the sheath electric field is a basic assumption of the dual-frequency analytical model. In the dual-frequency PIC simulation, the trajectory of a few thousand ions are saved, out of which a few ion trajectories show the signature of the reflection of ions. It is under these conditions that n_{sm} is determined not only by the ion flux injected from the boundary, but also by this flux of ions returning from the sheath.

In figure 10, case (a) shows that the ions propagate towards the sheath without any deflection in the bulk plasma, enter inside the sheath, accelerate and finally hit the electrode. The majority of ions in the PIC simulation shows this type of behaviour. Cases (b), (e), (g) and (i) show that the ions travel towards the sheath and reflect back at some point. These cases indicate that ions slow down while approaching towards the sheath region, stop for a while (trajectory is flat at the edge) and finally reflect back towards the bulk plasma. However, cases (e) and (i) indicate that the ions move outside the simulation region and cases (b) and (g) show that the ions remain in the simulation region after reflection. Cases (c), (d), (f) and (h) demonstrate that the ions move towards the sheath and reflect back at some point. After travelling a certain distance inside the bulk (opposite to sheath), the velocity becomes positive and it again moves towards the sheath and finally accelerates and hits the electrode. It is to be noted that the distance travelled inside the bulk after reflection is different in these cases. The only reason behind this ion reflection is the presence of strong field reversals at the time of low-frequency sheath expansion and collapse.

Figure 11 shows the spatiotemporal profile of the electric field for $J_{lf} = 3.6\,A\,m^{-2}$ and $J_{hf} = 26.4\,A\,m^{-2}$. In this figure, the field reversal regions are clearly observed at multiple times of an RF period near to the sheath region. The most probable reason for this field reversal is the electron fluid compression and rarefaction while the high-frequency sheath (which is modulated on low frequency) expands and collapses. Here because of ion reflection phenomena, there is a density jump in the bulk plasma from 1×10^{15} to $1.27 \times 10^{15}\,m^{-3}$. Figure 12 shows the time-averaged ion and snapshots of electron density profile for $J_{lf} = 3.3\,A\,m^{-2}$ and $J_{lf} = 3.6\,A\,m^{-2}$ at density $1 \times 10^{15}\,m^{-3}$. It is clear from figure 12 that the density jumps from 1×10^{15} to $1.27 \times 10^{15}\,m^{-3}$ when J_{lf} varies from 3.3 to $3.6\,A\,m^{-2}$ at a constant J_{hf}, i.e. $26.4\,A\,m^{-2}$.

Equation (14) shows that the stochastic heating is a function of density. However, this density is either considered as the bulk density or the density at the ion-sheath–plasma boundary. The density distribution inside the simulation region significantly changed for these two cases. The calculated ion density at the sheath edge by knowing n_w (ion density at the electrode) is $7.657 \times 10^{14}\,m^{-3}$ for $J_{lf} = 3.6\,A\,m^{-2}$. For $J_{lf} = 3.6\,A\,m^{-2}$, the analytical and simulation stochastic heatings are $S_{stocUL} = 196.835\,W\,m^{-2}$ and $S_{stocDF} = 247.3466\,W\,m^{-2}$, respectively. On the other hand, analytical stochastic heating calculated by considering 'bulk density' is $S_{stocUL} = 75.6478\,W\,m^{-2}$. These results are tabulated in table 1. Here the heating predicted by the dual-frequency analytical model is significantly less than the heating calculated by the PIC simulation because of the density jump inside the bulk plasma. Normally the analytical stochastic heating does not vary much either taking ion density from the bulk plasma or at the ion-sheath edge. Here, due to a density jump inside the bulk plasma the velocity amplitude of the bulk motion $u_{bh} = J_{hf}/en_0$ and H_{lf} drops significantly, as a result analytical heating prediction is significantly reduced. Here n_0 is the bulk density.

This indicates that the electron dynamics of the heating mechanism is different for these cases where strong field

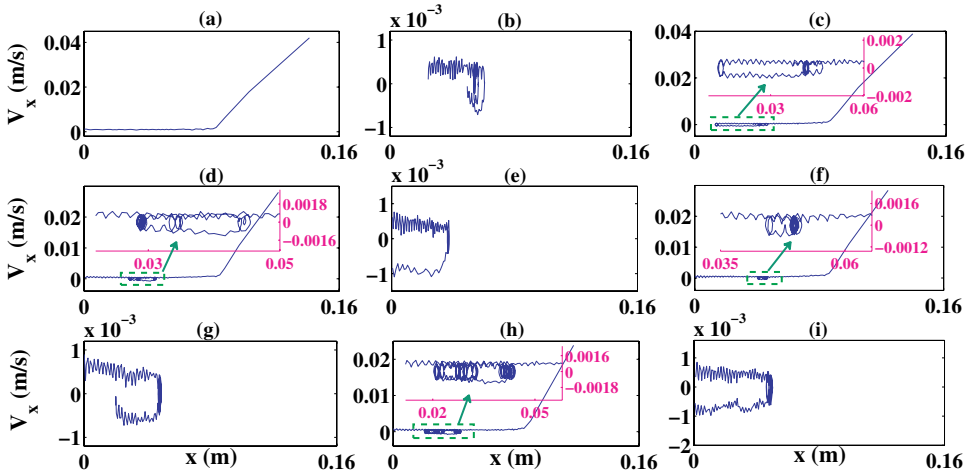

Figure 10. Trajectories of ions in the velocity phase space. In (*c*), (*d*), (*f*) and (*h*) the zoomed part of the figure is also shown where ion trajectories are clearly visualized. Conditions: argon gas, $J_{lf} = 3.6\,\mathrm{A\,m^{-2}}$, $J_{hf} = 26.4\,\mathrm{A\,m^{-2}}$, $T_e = 2.5\,\mathrm{eV}$, $T_i = 0.03\,\mathrm{eV}$, $f_{lf} = 1.695\,\mathrm{MHz}$, $f_{hf} = 27.12\,\mathrm{MHz}$.

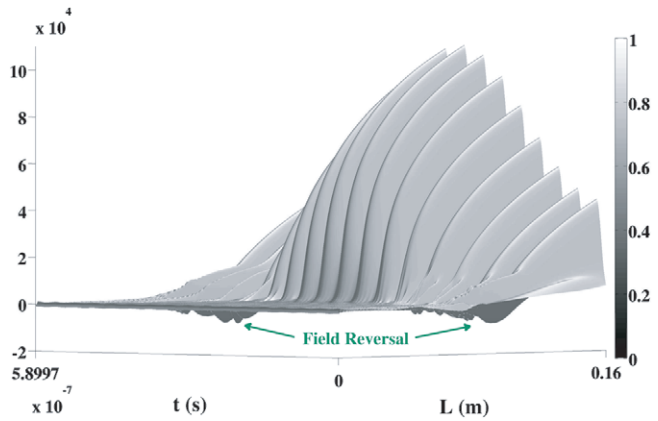

Figure 11. Spatiotemporal profile (surface plot) of electric field. Conditions: argon gas, $J_{lf} = 3.6\,\mathrm{A\,m^{-2}}$, $J_{hf} = 26.4\,\mathrm{A\,m^{-2}}$, $T_e = 2.5\,\mathrm{eV}$, $T_i = 0.03\,\mathrm{eV}$, $f_{lf} = 1.695\,\mathrm{MHz}$, $f_{hf} = 27.12\,\mathrm{MHz}$ at the density of $1 \times 10^{15}\,\mathrm{m^{-3}}$.

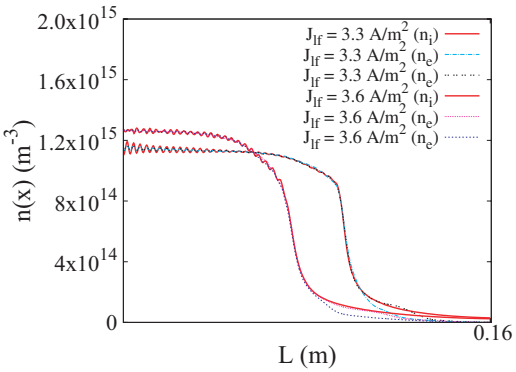

Figure 12. Ion and electron density profile for $J_{lf} = 3.3\,\mathrm{A\,m^{-2}}$ and $J_{lf} = 3.6\,\mathrm{A\,m^{-2}}$ at density $1 \times 10^{15}\,\mathrm{m^{-3}}$. The value of $J_{hf} = 26.4\,\mathrm{A\,m^{-2}}$ is the same in both cases. Conditions: argon gas, $T_e = 2.5\,\mathrm{eV}$, $T_i = 0.03\,\mathrm{eV}$, $f_{lf} = 1.695\,\mathrm{MHz}$, $f_{hf} = 27.12\,\mathrm{MHz}$.

reversal region is present and ion reflection phenomenon comes in picture. So the existing dual-frequency analytical model is not applicable for these cases.

4. Heating in dual-frequency is much higher than the frequencies acting alone

In the literature, Turner and Chabert [12] reported that the stochastic heating yielded by the superposition of low- and high-frequency currents (i.e. J_{lf} and J_{hf}) with different frequencies (*i.e.* f_{lf} and f_{hf}) can be much higher than the heating produced by either low current (J_{lf}) with low frequency (f_{lf}) or high current (J_{hf}) with high frequency (f_{hf}) acting alone. However, these results are in contrast to the additive effect reported by Kim *et al* [9]. The physical parameters used here are $T_e = 2.5\,\mathrm{eV}$, $T_i = 0.003\,\mathrm{eV}$, $f_{lf} = 1.695 \times 10^6\,\mathrm{Hz}$, $f_{lf} = 27.16 \times 10^6\,\mathrm{Hz}$ and the density is $6 \times 10^{14}\,\mathrm{m^{-3}}$. The low- and high-current density amplitudes are $J_{lf} = 2.1\,\mathrm{A\,m^{-2}}$ and $J_{hf} = 16.8\,\mathrm{A\,m^{-2}}$, respectively. Our PIC simulation indicates

Table 1. Stochastic heating (both analytical and simulation) for the case of $J_{lf} = 3.6\,\mathrm{A\,m^{-2}}$ and $J_{hf} = 26.4\,\mathrm{A\,m^{-2}}$ at density $1 \times 10^{15}\,\mathrm{m^{-3}}$.

J_{lf}	$(S_{stocUL})_{theory}$ (ion-sheath edge density)	$(S_{stocUL})_{theory}$ (bulk density)	$(S_{stocDF})_{simulation}$
$3.6\,\mathrm{A\,m^{-2}}$	$196.835\,\mathrm{W\,m^{-2}}$	$75.6478\,\mathrm{W\,m^{-2}}$	$247.3466\,\mathrm{W\,m^{-2}}$

that the stochastic heating may be significantly enhanced when two frequencies act together.

Figure 13 shows the PIC simulation results which represent the stochastic heating produced by the combined frequencies and compared it with heating produced by each frequency effect separately. For the cases when only lower frequency and higher frequency is applied separately, the stochastic heating is $S_{lf} = -1.5963\,\mathrm{W\,m^{-2}}$ and $S_{hf} = 5.4698\,\mathrm{W\,m^{-2}}$, respectively. The negative heating shown in the case of lower frequency is due to the large number of electrons being lost to the electrode, this results in a loss of power that is greater than the stochastic heating at the sheath edge. When both frequencies act together, the

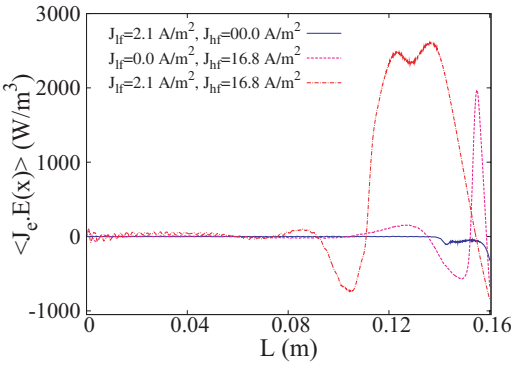

Figure 13. Time-averaged stochastic heating $\langle J_e.E\rangle$ for three different cases, i.e. the two frequencies acting separately and both acting together. Conditions: argon gas, $J_{lf} = 2.1\,A\,m^{-2}$, $J_{hf} = 16.8\,A\,m^{-2}$, $f_{lf} = 1.695\,MHz$, $f_{hf} = 27.12\,MHz$, $T_e = 2.5\,eV$, $T_i = 0.03\,eV$ at density $6 \times 10^{14}\,m^{-3}$.

stochastic heating produced is $S_{stocDF} = 71.457\,W\,m^{-2}$. It is clear here that the heating produced in the case when both frequencies act together is much higher (nearly 10 times) than the frequencies that act separately. There is little direct heating associated with the lower frequency, but in the presence of the lower frequency, the dynamic range of plasma density in the sheath region is considerably increased, and this indirectly causes the enhancement of the collisionless heating effect.

Turner and Chabert [12] first reported this effect for the case of fixed ions and the numerical results are also compared with the heating predicted by the analytical fluid model.

5. Conclusion and discussion

Using analytic and self-consistent particle-in-cell models, the electron dynamics inside a sheath region of a dual-frequency RF capacitive discharge have been investigated in connection with the collisionless heating through the Fermi acceleration mechanism. Stochastic heating in dual frequency is controlled mainly by six scaling parameters (i.e. J_{lf}, J_{hf}, T_e, ω_{lf}, ω_{hf} and n_{sm}). There are different ways of scaling these parameters and two different approaches are discussed here.

In the *first approach* benchmarking of the dual-frequency analytical model is the same as that used by Kawamura *et al* [10] where H_{lf} is calculated by varying J_{lf} and n_{sm} simultaneously. However in Kawamura *et al* [10] simulation, the number of data points are rather small, i.e. $H \sim 5.0$–8.2. Present simulation results widen the range of H_{lf}, i.e. $H_{lf} \sim 1.77$–29.2 which are in fair agreement with the dual-frequency analytical model given by Kawamura *et al* [10] which is the extension of the single-frequency analytical model given by Kaganovich *et al* [21]. Here the lower and higher frequency current drive amplitudes are varied from $J_{lf} = 0.5$ to $11.12\,A\,m^{-2}$ and $J_{hf} = 4.0$ to $88.96\,A\,m^{-2}$ at the corresponding densities of 1.1×10^{14}–$4 \times 10^{15}\,m^{-3}$. The ratio of $J_{hf}/J_{lf} = 8$ for all set of simulations.

In the *second approach* the stochastic heating is studied by keeping the density constant and by varying the ratio of J_{hf}/J_{lf}, by changing the lower current density amplitude J_{lf}. Stochastic heating at two different densities, i.e. $5 \times 10^{14}\,m^{-3}$ and $1 \times 10^{15}\,m^{-3}$ has been investigated. At a constant density the simulation results agree with the dual-frequency analytical model given by Kawamura *et al* [10] in a certain range of H_{lf}. It is observed that H_{lf} is in fair agreement with the dual-frequency analytical model, given by Kawamura *et al* [10], for the range 5.8–9.0 and 9.4–12.35 at the densities of $5 \times 10^{14}\,m^{-3}$ and $1 \times 10^{15}\,m^{-3}$, respectively. The presence of strong field reversal regions are identified at the time of low-frequency sheath expansion and collapse. The most probable reason for the field reversal regions at multiple times during an RF period is electron fluid compression and rarefaction while the high frequency (which is modulated on the low frequency) expands and collapses. The signature of ion reflection is also observed above the upper critical limit of H_{lf} because of the presence of strong field reversal regions.

The stochastic heating produced by the combined frequencies, i.e. f_{lf} and f_{hf}, and heating produced by each frequency effect separately has been compared with the PIC simulation. The PIC results indicates that the stochastic heating is significantly enhanced when two frequencies act together.

Stochastic heating in the case of dual-frequency capacitive discharges depends on various discharge parameters and the validation of dual-frequency analytical model given by Kawamura *et al* [10] has been studied by scaling of these parameters. For intermediate values of H_{lf}, the dual-frequency analytical model is satisfactory. However, the new physical effects (such as strong field reversal and reflection of ions) appear for higher H_{lf} and the PIC results deviate from the existing dual-frequency analytical model. In most experiments $H_{lf} \sim 5$ and these effects are not observed there. On the other side for lower H_{lf}, the existing analytical models agree well with the net heating observed in simulations, which includes electron loss effects. In global models, for example, the latter effect should not be included separately in conjunction with these heating models.

Acknowledgment

This research is based upon works supported by Science Foundation Ireland under Grant No 07/IN.1/1907 and 08/SRC/I1411.

References

AQ2

[1] Goto H H, Lowe H D and Ohmi T 1992 Dual excitation reactive ion etcher for low energy plasma processing *J. Vac. Sci. Technol.* A **10** 3048
[2] Goto H H, Lowe H D and Ohmi T 1993 Independent control of ion density and ion bombardment energy in a dual RF excitation plasma *IEEE Trans. Semicond. Manuf.* **6** 58
[3] Rauf S and Kushner M J 1999 Nonlinear dynamics of radio frequency plasma processing reactors powered by multifrequency sources *IEEE Trans. Plasma Sci.* **27** 1329
[4] Robiche J, Boyle P C, Turner M M and Ellingboe A R 2003 Analytical model of a dual frequency capacitive sheath *J. Phys. D: Appl. Phys.* **36** 1810
[5] Lieberman M A and Lichtenberg A J 2005 *Principles of Plasma Discharges and Materials Processing* (New York: Wiley)

[6] Perret A, Chabert P, Jolly J and Booth J P 2005 Ion energy uniformity in high-frequency capacitive discharges *Appl. Phys. Lett.* **86** 021501
[7] Jolly J and Booth J P 2005 Atomic hydrogen densities in capacitively coupled very high-frequency plasmas in H_2: effect of excitation frequency *J. Appl. Phys.* **97** 103305
[8] Boyle P C, Ellingboe A R and Turner M M 2004 Independent control of ion current and ion impact energy onto electrodes in dual frequency plasma devices *J. Phys. D: Appl. Phys.* **37** 697
[9] Kim H C, Lee J K and Shon J W 2003 Analytic model for a dual frequency capacitive discharge *Phys. Plasmas* **10** 4545
[10] Kawamura E, Lieberman M A and Lichtenberg A J 2006 Stochastic heating in single and dual frequency capacitive discharges *Phys. Plasmas.* **13** 053506
[11] Turner M M and Chabert P 2006 Electron heating mode transitions in dual frequency capacitive discharges *Appl. Phys. Lett.* **89** 231502
[12] Turner M M and Chabert P 2006 Collisionless heating in capacitive discharges enhanced by dual-frequency excitation *Phys. Rev. Lett.* **96** 205001
[13] Turner M M and Chabert P 2007 Electron heating mechanisms in dual-frequency capacitive discharges *Plasma Sources Sci. Technol.* **16** 364
[14] Turner M M 2009 Collisionless heating in radio-frequency discharges: a review *J. Phys. D: Appl. Phys.* **42** 194008
[15] Chabert P, Levif P, Raimbault J L, Rax J M, Turner M M and Lieberman M A 2006 Electron heating in multiple-frequency capacitive discharges *Plasma Phys. Control. Fusion* **48** B231
[16] Gozadinos G, Turner M M and Vender D 2001 Collisionless electron heating by capacitive rf sheaths *Phys. Rev. Lett.* **87** 135004
[17] Kaganovich I D 2002 Anomalous capacitive sheath with deep radio-frequency electric-field penetration *Phys. Rev. Lett.* **89** 265006
[18] Godyak V A 1972 Statistical heating of electrons at an oscillating plasma boundary *Sov. Phys.—Tech. Phys.* **16** 1073
[19] Lieberman M A 1988 Analytical solution for capacitive RF sheath *IEEE Trans. Plasma Sci.* **16** 638
[20] Gozadinos G, Vender D and Turner M M 2001 Boundary conditions and particle loading for the modeling of a semi-infinite plasma *J. Comput. Phys.* **172** 348
[21] Kaganovich I D, Polomarov O V and Theodosiou C E 2006 Revisiting the anomalous RF field penetration into a warm plasma *IEEE Trans. Plasma Sci.* **34** 696
[22] Sharma S and Turner M M 'Simulation study of stochastic heating in single frequency capacitively coupled discharges with critical evaluation of analytical models' *Plasma Sources Sci. Technol.* sublitted
[23] Brinkmann R P 2007 Beyond the step model: approximate expressions for the field in the plasma boundary sheath *J. Appl. Phys.* **102** 093303
[24] Brinkmann R P 2009 From electron depletion to quasi-neutrality: the sheathbulk transition in rf modulated discharges *J. Phys. D: Appl. Phys.* **42** 194009
[25] Polomarov O, Theodosiou C E and Kaganovich I D 2005 Enhanced collisionless heating in a nonuniform plasma at the bounce resonance condition *Phys. Plasmas* **12** 80704

AQ3

QUERIES

Page 1
AQ1
Please be aware that the colour figures in this article will only appear in colour in the web version. If you require colour in the printed journal and have not previously arranged it, please contact the Production Editor now.

Page 8
AQ2
Please check the details for any journal references that do not have a blue link as they may contain some incorrect information. Pale purple links are used for references to arXiv e-prints.

Page 9
AQ3
Please provide year, volume number and page range for Ref. [22].